

523-24

410703

313

N95-22460

395846

Forced free-shear layer measurements

By R. L. LeBoeuf

Detailed three-dimensional three-component phase averaged measurements of the spanwise and streamwise vorticity formation and evolution in acoustically forced plane free-shear flows have been obtained. For the first time, phase-averaged measurements of all three velocity components have been obtained in both a mixing layer and a wake on three-dimensional grids, yielding the spanwise and streamwise vorticity distributions *without invoking Taylor's hypothesis*. Initially, two-frequency forcing was used to phase-lock the roll-up and first pairing of the spanwise vortical structures in a plane mixing layer. The objective of this study was to measure the near-field vortical structure morphology in a mixing layer with "natural" laminar initial boundary layers. For the second experiment the second and third subharmonics of the fundamental roll-up frequency were added to the previous two-frequency forcing in order to phase-lock the roll-up and first *three* pairings of the spanwise rollers in the mixing layer. The objective of this study was to determine the details of spanwise scale changes observed in previous time-averaged measurements and flow visualization of unforced mixing layers. For the final experiment, single-frequency forcing was used to phase-lock the Karman vortex street in a plane wake developing from nominally two-dimensional laminar initial boundary layers. The objective of this study was to compare measurements of the three-dimensional structure in a wake developing from "natural" initial boundary layers to existing models of wake vortical structure.

Part 1: Forced mixing layers

1. Motivation and objectives

The three-dimensional structure of plane transitioning mixing layers has been the subject of many experimental and computational studies since the early seventies when it was realized that, in addition to spanwise vortices ("rollers") which arise as a result of the Kelvin-Helmholtz instability, a secondary structure was also generated. The secondary structure took the form of "spatially-stationary" streamwise vortices which were soon identified in flow visualization studies and in velocity measurements. These earlier results showed that the streamwise structures ("ribs") first formed in the *braid* region, a region connecting adjacent spanwise vortices, and that their locations were related to the strength and position of (weak) incoming disturbances.

The presence and role of these "naturally-occurring" streamwise structures were recently investigated through detailed time-averaged measurements (Bell and Mehta 1992). A plane, two-stream mixing layer was generated with nominally two-dimensional laminar initial boundary layers. The measurements indicated that

small spanwise disturbances originating upstream in the boundary layer flow were amplified, leading to the formation of spatially-stationary streamwise vortices. Based on mean velocity measurements in the near-field region, it was concluded that this amplification occurred just downstream of the first spanwise vortex roll-up. The mean vorticity first appeared in "clusters" containing vorticity of both signs, but further downstream, it "re-aligned" to form counter-rotating pairs in a nominally linear arrangement. The vortex structure was found to grow in size with downstream distance, the spanwise wavelength associated with them increasing in a stepwise fashion. In contrast to some other experimental results, however, a jump in spanwise wavelength was *not* observed at *every* estimated roller pairing location and the spanwise wavelength remained constant over fairly large streamwise distances. Since the jumps in spanwise scale were correlated with local increases in the average streamwise circulation per vortex, Bell & Mehta (1992) suggested that at least one mechanism for the increase in spanwise scale was amalgamation of vortices of the same sign.

Although the secondary structure in a plane mixing layer has already received considerable attention, all issues regarding the three-dimensional structure in "natural" mixing layers have not yet been addressed. In terms of the computations, limits imposed by boundary conditions and the expense associated with grid size and computation time make it difficult to evaluate the structure of a (natural) spatially-developing mixing layer. Of course, details and interactions of the secondary structure are lost through time-averaging while the use of partial vorticity and Taylor's hypothesis, which were commonly used to interpret previous measurements, obviously add to the uncertainty in experimental results. In fact, the measurements described in this report were used to show that the use of Taylor's hypothesis introduces large errors both in the shapes and levels of the vorticity contours, especially in the roller pairing regions (LeBoeuf & Mehta 1994*a*). The issue of spanwise scale change of the streamwise vortical structures in mixing layers has also already received considerable attention, but it is still not clear when and how such a scale change will occur in a "natural" mixing layer. In particular, details of the streamwise structure scale change have not been studied quantitatively in experiments.

The main objective of the first study described in this report was to investigate the development of three-dimensionality and evolution through a spanwise roller pairing in a forced plane two-stream mixing layer developing from "natural" laminar boundary layers. Acoustic forcing was used to phase-lock the initial roll-up and first-pairing, which would otherwise occur randomly in an unforced mixing layer. Phase-averaged measurements were then used to quantify the resulting vorticity development and interaction (LeBoeuf & Mehta 1994*b*). Since a spanwise scale change was not observed through the first pairing, a second study was conducted in which acoustic forcing was used to phase-lock the formation and first *three* pairings of the spanwise rollers. Phase-averaged vorticity measurements were then used to identify the regions and details of the spanwise scale changes. The mechanisms responsible for the scale changes in this "natural" mixing layer have also been

identified (LeBoeuf & Mehta 1994c).

2. Accomplishments

2.1 The experiment

The experimental apparatus was essentially the same as that described in LeBoeuf (1993) and has been further described in detail in LeBoeuf & Mehta (1994b); only a brief description is therefore given here. The experiments were conducted in a mixing layer wind tunnel with the two free-stream velocities set to 12 m/s and 7.2 m/s. The boundary layers on the splitter plate were laminar and nominally two-dimensional with these operating velocities. Velocity measurements were made using a single cross-wire probe which was rotated in order to obtain data in two-coordinate planes (uv and uw).

The forcing signals used to obtain the results described in this report consisted of the sum of a sine wave at the fundamental “most-probable” roll-up frequency (500 Hz, obtained from centerline spectra in the unforced layer) and its first subharmonic (250 Hz). Two additional subharmonics (125 Hz and 62.5 Hz) were added for the second (spanwise scale change) study. The forcing signal relative phase angles were optimized in order to induce rolling-type interactions for all pairings. The individual sine waves were combined using a simple summing circuit and output via an audio amplifier to speakers which were placed directly across from the splitter plate trailing edge at a side-wall slot location. The amplitude (volume) of the output signal from the amplifier was set to the absolute minimum level that still gave adequate coherence in the phase-locking.

For the phase-averages obtained in the first study, 768 ensembles of 16 samples per cycle were measured. The measurement grid consisted of 55 uniformly spaced X locations in the range 1 to 28 cm and 20 uniformly spaced Y locations distributed over a linearly increasing range of -1 to 1 cm at $X = 1$ cm to -2.5 to 2.5 cm at $X = 28$ cm. In the spanwise direction, the three-dimensional grid ranged from $Z = -5$ to 5 cm with 41 uniformly spaced locations. For the phase-averages obtained in the second study, 768 ensembles of 32 samples per cycle were measured. The measurement grid consisted of 155 uniformly spaced X locations in the range 1 to 78 cm and 11 uniformly spaced Y locations distributed over a linearly increasing range of $-$ to 1 cm at $X = 1$ cm to -6.2 to 4.4 cm at $X = 78$ cm. In the spanwise direction, the three-dimensional grid ranged from $Z = 0$ to 5 cm with 21 uniformly spaced locations.

2.2 Results and discussion

2.2.1 Two-frequency forcing: initial roll-up and first pairing

The streamwise evolution of spanwise vorticity along the mixing layer centerline ($Z = 0$) is depicted in Figs. 1(a-d) for four phases (or times). In effect, every fourth phase out of the 16 measured phases per subharmonic cycle is presented. The evolution and pairing of sets of primary rollers can be easily tracked through the four phases shown. The initial spanwise vortex roll-up occurs at $X \approx 5$ cm. Clearly, signs of subharmonic forcing are present early in the mixing layer development

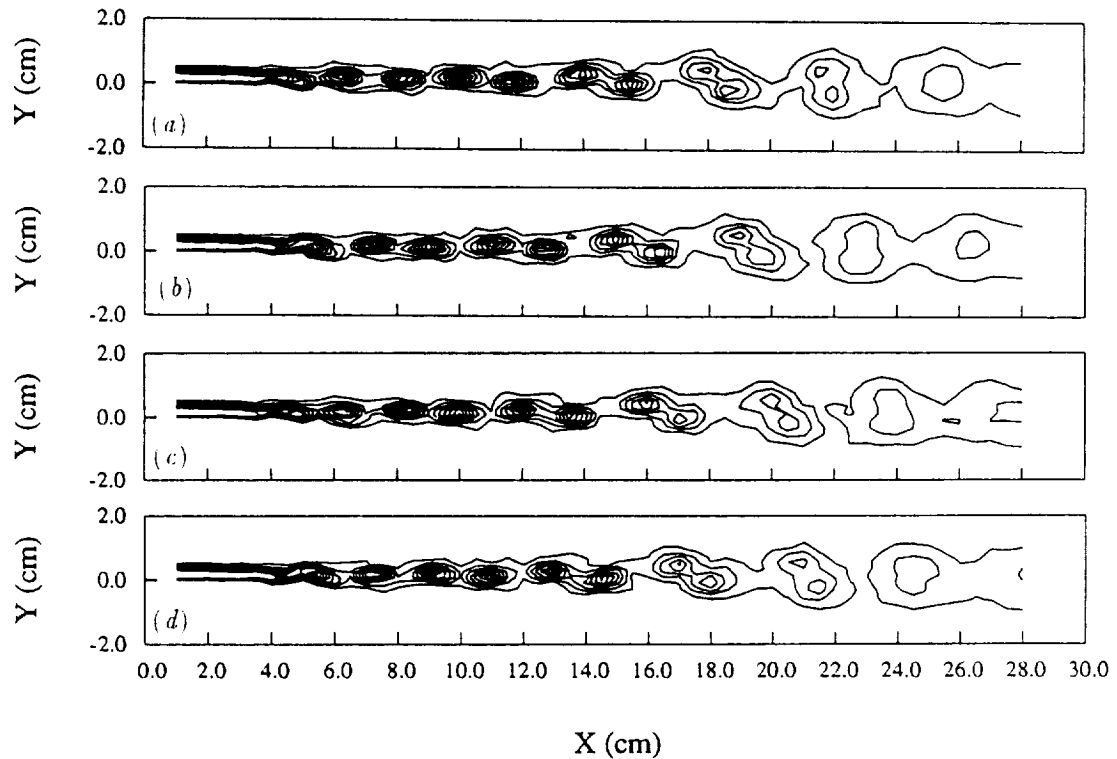


FIGURE 1. Centerplane phase-averaged spanwise vorticity ($\langle \Omega_z \rangle / U_0$, cm^{-1}) contours at various phases. Lowest level = -0.25 , increment = -0.5 . (a) phase 1; (b) phase 5; (c) phase 9; (d) phase 13.

since distinguishable *pairs* of primary rollers are discernable from the onset of their development. Spanwise vortices of each pair start to move closer together between $X \approx 10$ and 15 cm, begin to corotate at $X \approx 15$ cm, and complete the first pairing by $X \approx 25$ cm. The peak phase-averaged spanwise vorticity levels drop by an order of magnitude during the pairing process.

Details of the vortical structures can be examined in detail by using two-dimensional “cuts” through the three-dimensional data. To maintain figure legibility, the figures and discussion thereof was divided into two parts: the initial spanwise vortex roll-up region and the pairing region. In the initial roll-up region, spanwise vorticity contours in XY -planes which intersect ribs (Figs. 2a and c) and those between ribs (e.g. Fig. 2b) appear quite similar both in terms of qualitative (structural) features and vorticity levels. The cups of intense spanwise vorticity observed by Buell & Mansour (1989a) and Rogers & Moser (1992) in their direct numerical simulation studies were not found in the present investigation. The formation of cups was attributed to the effects of alternating stretching and compression of the primary rollers by collapsed rib vortices.

The XY -planes of streamwise vorticity through the ribs and between them, on

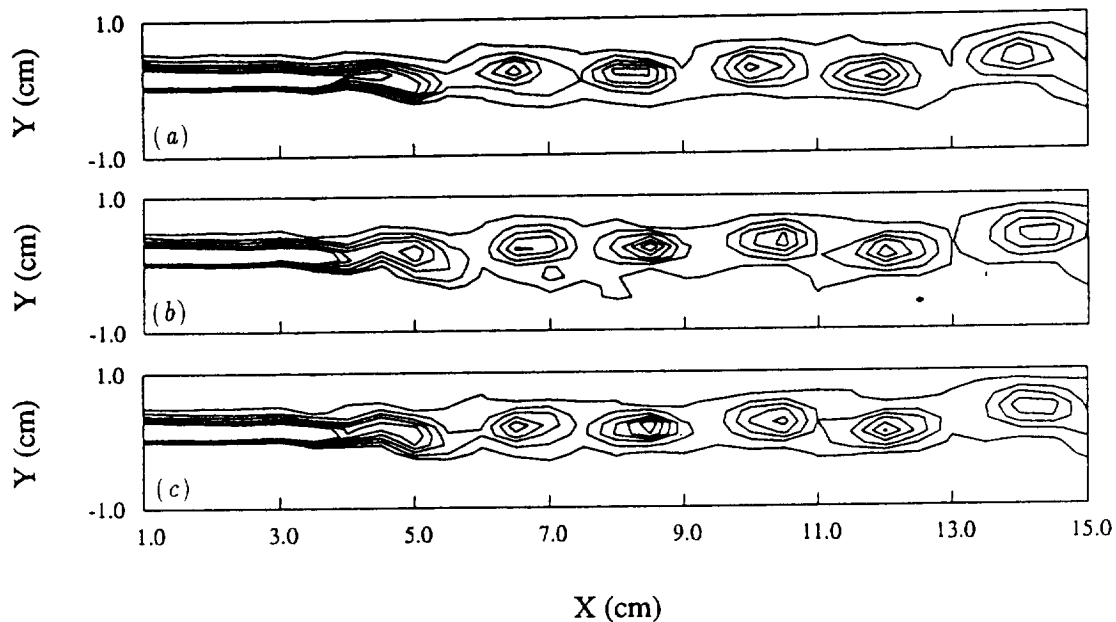


FIGURE 2. Phase-averaged spanwise vorticity ($\langle \Omega_z \rangle / U_0$, cm^{-1}) contours at phase 1. Lowest level = -0.25 , increment = -0.75 . (a) *RP* through positive rib, $Z = 0.25$ cm; (b) *BP*, $Z = 1.25$ cm; (c) *RP* through negative rib, $Z = 2$ cm.

the other hand, certainly show some obvious differences. In addition to the rib vortices, *opposite-sign* streamwise vorticity peaks appear within the spanwise roller core in planes intersecting the ribs (Figs. 3*a* and *c*). This effect is attributable to (streamwise) kinking of the spanwise roller, and its appearance here is consistent with the simulation results of Buell & Mansour (1989*a*) and Rogers & Moser (1992) and with the measurements of Lasheras & Choi (1988), Tung (1992) and Nygaard & Glezer (1991). This production of opposite-signed streamwise vorticity has been explained in vortex stretching terms in the streamwise vorticity equation by Buell (1991) and Rogers & Moser (1991). Since the deflection of the spanwise roller reaches a maximum and therefore has only a spanwise component between the ribs ($Z = 1.25$ cm), its contribution is absent in that plane (Fig. 3*b*). The arrangement of rib vortices and streamwise vorticity within the spanwise roller yields a three-tier arrangement of streamwise vorticity in cross-stream (YZ)-planes which intersect the primary rollers (Fig. 4*a*), whereas only the rib vortices are apparent in the cross-stream planes which intersect the braid regions (Fig. 4*b*).

In the pairing region, evolution of the streamwise vorticity was first examined through cross-stream (YZ -plane) cuts. Figs. 5(*a*) and (*b*) correspond to planes which intersect the primary (paired) rollers at $X = 22$ and 26 cm, respectively. It is evident from Fig. 1 that pairing is occurring between approximately $X = 17$ cm and $X = 24$ cm. A comparison of Figs. 5(*a*) and (*b*) indicates that reorganization

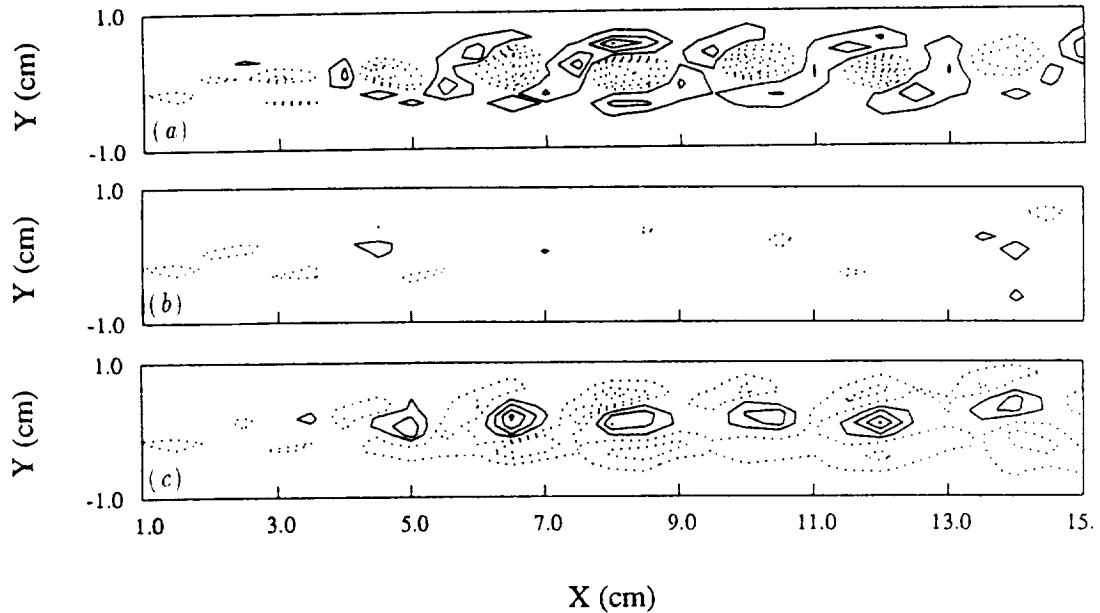


FIGURE 3. Phase-averaged streamwise vorticity ($\langle \Omega_x \rangle / U_0$, cm^{-1}) contours at phase 1. Negative \cdots , positive — , lowest level = ± 0.2 , increment = ± 0.3 . (a) *RP* through positive rib, $Z = 0.25$ cm; (b) *BP*, $Z = 1.25$ cm; (c) *RP* through negative rib, $Z = 2$ cm.

(interaction) of the secondary vorticity continues to take place even towards the final stages of pairing. In particular, it appears that the streamwise vorticity arrangement is tending toward the three-tier arrangement within a cycle after pairing occurs (Fig. 5*b*).

Figs. 6(*a*) and (*b*) correspond to YZ -planes which intersect the braid regions at $X = 20.5$ and 23.5 cm, respectively. In contrast to the near-field downstream of $X \approx 20$ cm, the peak streamwise vorticity levels become higher in the braid region. Most importantly, the spanwise scale or spacing of the rib vortices has *not* increased through this first pairing. Thus, compared to the near-field value, the spanwise to streamwise wavelength ratio was decreased from about 1.3 to 0.65.

In the pairing and post-pairing stages of the mixing layer, exemplary XY -plane cuts of spanwise and streamwise vorticity through ribs and between ribs are shown in Figs. 7 and 8, respectively. As in the upstream domain, cuts showing spanwise vorticity contours through the ribs and between them appear very similar and, even in this region, there are no signs of the cups of relatively strong spanwise vorticity reported for the simulation results (Buell & Mansour 1989*a*; Rogers & Moser 1992).

As expected, the streamwise vorticity is significantly weaker in planes between ribs compared to those through the ribs. The two rollers undergoing pairing clearly exhibit the three-tier distribution as they start to rotate about each other. As

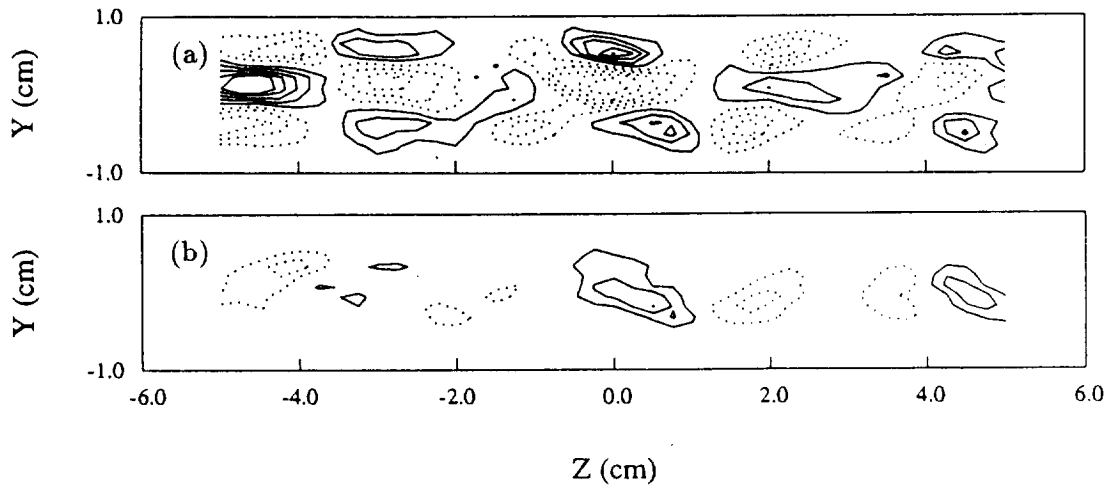


FIGURE 4. Cross-stream plane phase-averaged streamwise vorticity ($\langle \Omega_x \rangle / U_0$, cm^{-1}) contours at phase 1. Negative , positive ——— , lowest level = ± 0.2 , increment = ± 0.2 . (a) $X = 8$ cm; (b) $X = 5.5$ cm.

they pair, the two regions of spanwise roller core vorticity eventually coalesce, thus forming the contribution from the new core. In following the evolution of the perishing braid regions, the rib vorticity in between the two pairing rollers seemed to “disappear”. Simulation results suggest that this vorticity is destroyed by intense vortex stretching in this region (Moser & Rogers 1993).

Note that once the pairing process is complete ($X \approx 25$ cm), the streamwise vorticity of the rib vortices is substantially higher than that due to kinking of the primary rollers. In addition, the rib contribution to the streamwise vorticity is higher in the braid than it is in the primary roller YZ -planes. This is in sharp contrast to the initial roll-up region, where the streamwise vorticity levels in the primary roller cores due to their kinking are comparable to those of the rib contribution, which in turn is higher in the rollers compared to its magnitude in the braids. The same trends were apparent in the experimental results of Tung (1992) and in the temporal simulation results of Moser & Rogers (1993). Decreased kinking of the rollers is at least partly responsible for this observed effect since the paired structure is more two-dimensional than the pre-paired rollers. On examining XY -plane cuts in the region surrounding the ribs, it was found that the ribs are still wrapped around the rollers, but the ends are skewed in the spanwise direction, thus reducing their streamwise vorticity contribution in YZ -planes which intersect the primary rollers.

The phase-averaged vorticity measurements confirm that relatively strong streamwise vorticity appears in mixing layers as a result of an amplification of small incoming disturbances — it is *not* just directly fed-in from the boundary layers. The streamwise vorticity is first observed in the form of ribs just upstream of where the

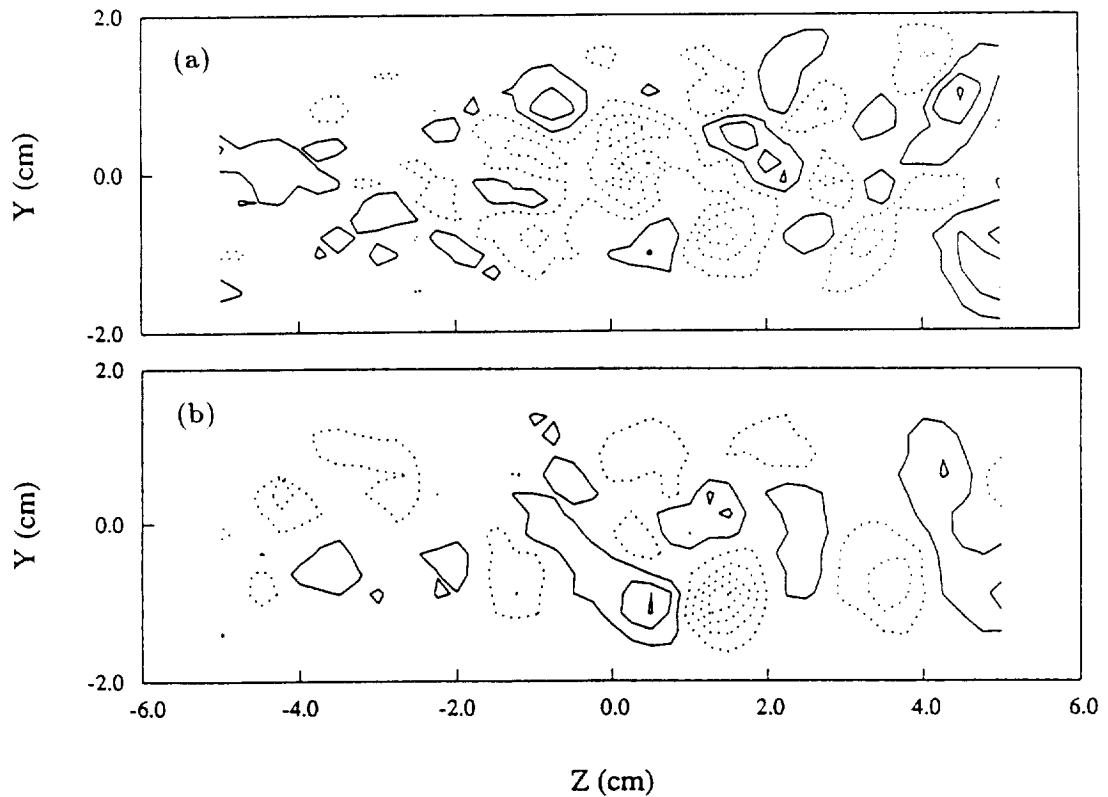


FIGURE 5. Cross-stream plane phase-averaged streamwise vorticity ($\langle \Omega_x \rangle / U_0$, cm^{-1}) contours at phase 1 through CPs. Negative , positive ——— , lowest level = ± 0.075 , increment = ± 0.15 . (a) $X = 22$ cm; (b) $X = 26$ cm.

first spanwise vortex is rolling-up. At the same time, the first spanwise roller becomes kinked, thus also contributing to the streamwise vorticity. As a result, cross-stream cuts through the braid regions show the familiar row of counter-rotating streamwise vortex pairs while those through the spanwise rollers exhibit a three-tier distribution consisting of the rib vortices aligned vertically with an opposite-signed contribution from the roller between them. This type of behavior and distribution are in agreement with previous observations in experiments (Tung 1992) and simulations (Buell & Mansour 1989*a*; Rogers & Moser 1992).

Because of the relatively strong contribution of the kinked rollers and the fact that the rib vortices are more aligned with the mean flow around the rollers, the highest levels of phase-averaged streamwise vorticity and circulation were observed in the spanwise vortex cores in the near-field region. The strong kinking of the spanwise rollers by the rib vortices was also observed in numerical simulations (Buell & Mansour 1989*a*; Rogers & Moser 1992). However, cups of relatively strong spanwise vorticity (also a result of the rib induced effects) reported for the simulation results

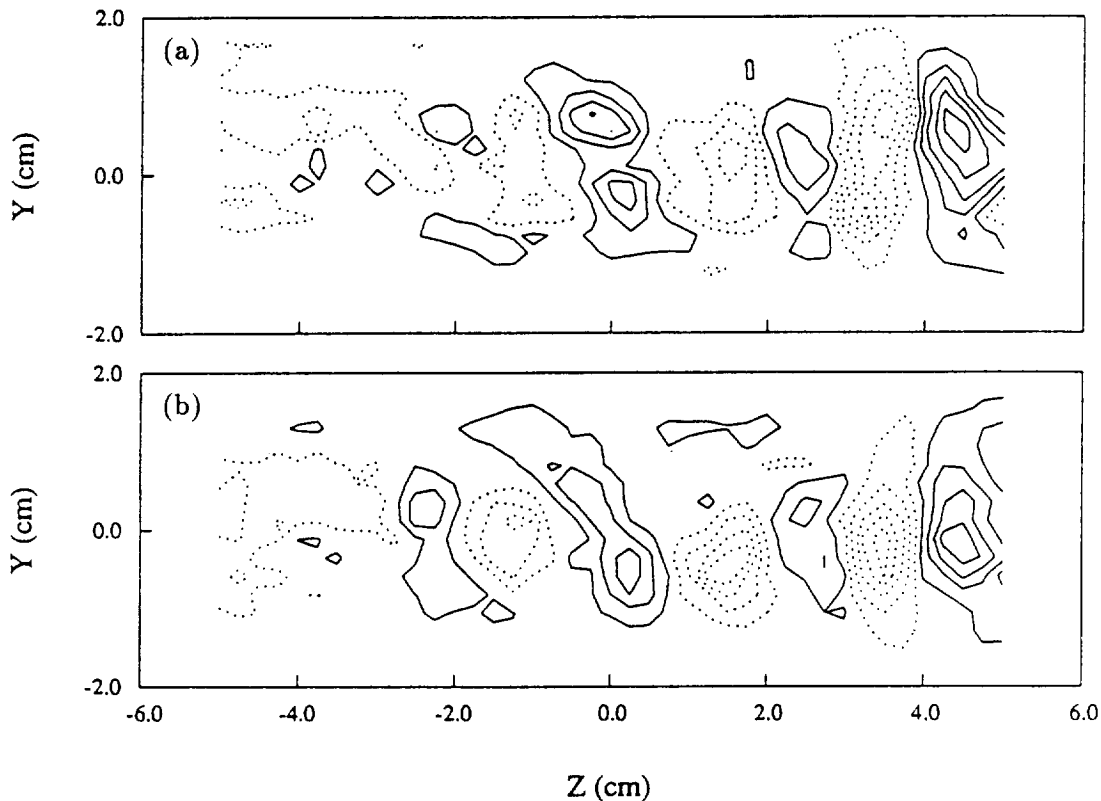


FIGURE 6. Cross-stream plane phase-averaged streamwise vorticity ($\langle \Omega_x \rangle / U_0$, cm^{-1}) contours at phase 1 through *MPs*. Negative \cdots , positive — , lowest level = ± 0.075 , increment = ± 0.15 . (a) $X = 20.5$ cm; (b) $X = 23.5$ cm.

were not observed in the present measurements. This is particularly surprising since the initial rib circulation in the present experiments is comparable to that used in the temporal simulations of Rogers & Moser (1992).

The morphology of the surviving braid region rib vortices was not significantly affected by the spanwise vortex pairing. In particular, their spanwise spacing did not increase after the pairing. This result is consistent with previous time-averaged measurements (Bell & Mehta 1992) which showed that the first increase in spacing did not occur until $X \approx 50$ cm, well downstream of the present measurement domain and after an estimated two spanwise vortex pairings had occurred. It also supports the findings of Rogers & Moser (1993), who suggested that the details of the spanwise scale change are dependent on the nature of the initial disturbance environment. The main effect noted in the post-pairing region is that the levels of streamwise vorticity in the roller core planes are reduced such that the highest levels are now found in the braid region. The smaller relative contribution due to kinking of the spanwise rollers is related to both, a reduction in roller kinking and a faster

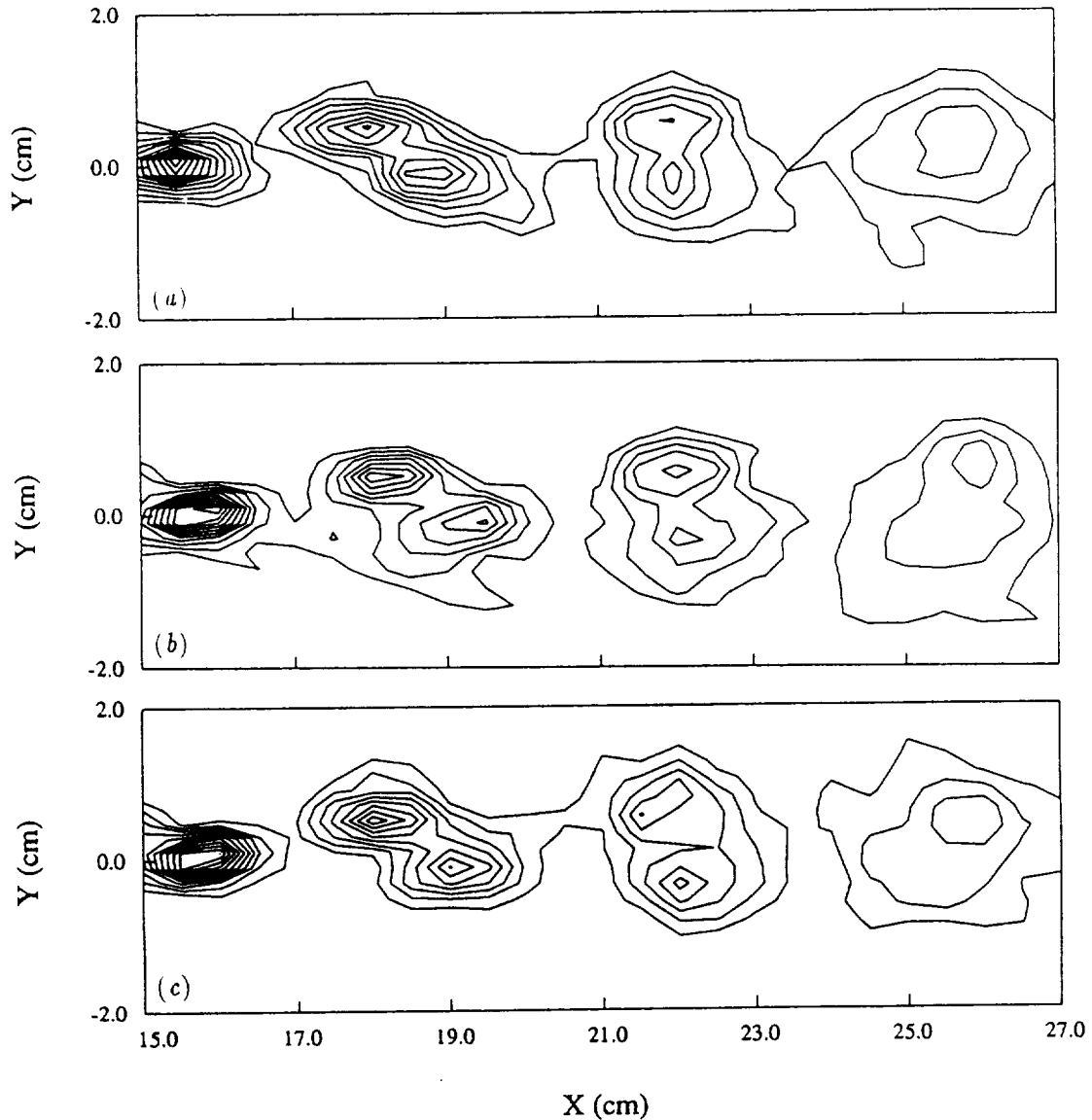


FIGURE 7. Phase-averaged spanwise vorticity ($\langle \Omega_z \rangle / U_0$, cm^{-1}) contours at phase 1. Lowest level = -0.25 , increment = -0.25 . (a) *RP* through positive rib, $Z = 0.25$ cm; (b) *BP*, $Z = 1$ cm; (c) *RP* through negative rib, $Z = 1.75$ cm.

rate of decay of the spanwise vorticity compared to that of the streamwise vorticity. The ribs make a smaller contribution in the roller planes because its ends are tilted in the spanwise direction. This change in the relative contributions is the reason why in the time-averaged measurements, the three-tier distribution observed in the near-field region soon "re-aligned" into a single row of mean streamwise vorticity (Bell & Mehta 1992).

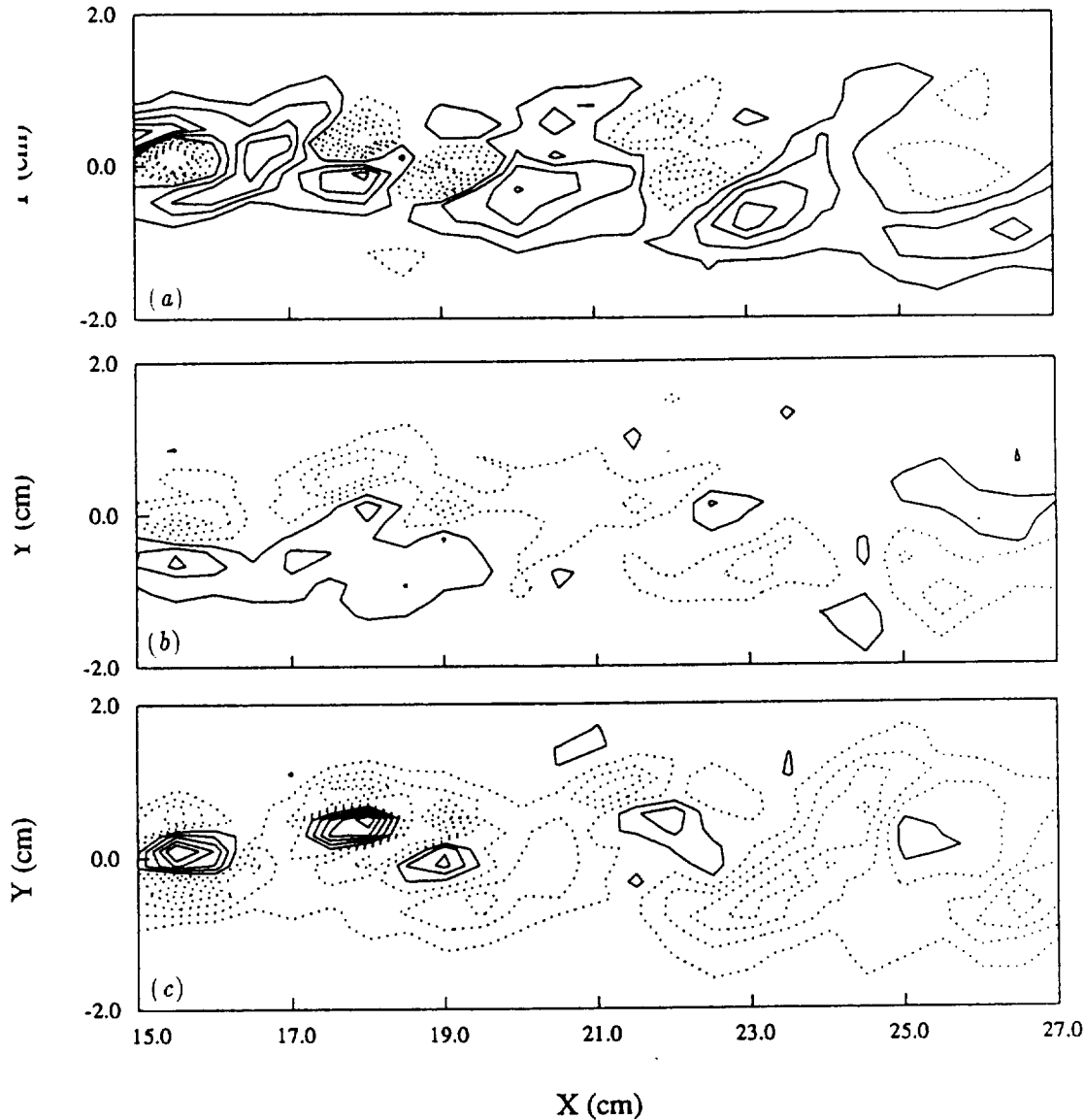


FIGURE 8. Phase-averaged streamwise vorticity ($\langle \Omega_x \rangle / U_0$, cm^{-1}) contours at phase 1. Negative \cdots , positive — , lowest level = ± 0.075 , increment = ± 0.15 . (a) *RP* through positive rib, $Z = 0.25$ cm; (b) *BP*, $Z = 1$ cm; (c) *RP* through negative rib, $Z = 1.75$ cm.

The present results clearly show that a plane mixing layer originating from laminar boundary layers will develop a three-dimensional structure in the form of streamwise vorticity as soon as the Kelvin-Helmholtz instability generates spanwise vortex rollers. Although in practice the details of the streamwise vortical structures will be facility dependent, they will generally appear in the form of an array of counter-rotating vortex pairs. The present data are consistent with existing models of the

secondary structure: rib vortices are formed in the braid region which wrap around the spanwise rollers (from the bottom of one roller to the top of the next). The streamwise vorticity and its associated effects on the mixing layer properties decay slowly with streamwise distance. This secondary structure therefore forms an integral and important part of the structural morphology of a transitioning mixing layer.

2.2.1 Four-frequency forcing: measurements of a spanwise scale change

The streamwise evolution of spanwise vorticity ($\langle \Omega_z \rangle / U_0$, cm^{-1}) along the mixing layer centerline ($Z = 0$) is depicted in Figs. 9(a-d) for four phases (or times). In effect, every eighth phase out of the 32 measured phases per lowest (third) subharmonic cycle is presented. The evolution and pairings of sets of primary rollers can be easily tracked through the four phases shown. The initial spanwise vortex roll-up occurs at $X \approx 5$ cm and the spanwise rollers are shed with an initial streamwise wavelength of about 1.75 cm. Clearly, signs of subharmonic forcing are present early in the mixing layer development since distinguishable *sets* of primary rollers are discernable at the onset of their development. Spanwise vortices of each pair start to move closer together between $X \approx 10$ and 15 cm, begin to corotate between $X \approx 15$ and 20 cm, and complete the first pairing by $X \approx 25$ cm. The second pairing is initiated immediately after the first pairing is complete, beginning between $X \approx 25$ and 30 cm and ending at $X \approx 50$ cm. The third pairing, which immediately follows, remains in progress up to the end of the measurement domain at $X = 78$ cm. The peak phase-averaged spanwise vorticity levels drop from 4 cm^{-1} to 1 cm^{-1} during the first pairing, down to 0.5 cm^{-1} during the second pairing, and finally down to 0.4 cm^{-1} during the third pairing.

Since the objective of the present study was to investigate spanwise scale changes associated with the rib structures, the spatial evolution of surviving rib structures was observed as they evolved through the three spanwise roller pairings. This is achieved by marching in X and phase at the same time. With 32 phases per third subharmonic forcing cycle ($1/62.5 \text{ Hz} = 0.016$ seconds duration), this gives a streamwise evolution of 0.48 cm per phase, based on an average convection velocity, $(U_1 + U_2)/2 = 9.6 \text{ m/s}$. Of course, as adjacent rollers pair, the braid region between them is engulfed into the new roller. Therefore, the so-called "surviving" braid region was chosen for examination of its streamwise evolution through the three roller pairings. The surviving braid region selected for the present scrutiny is marked by the first vertical line in Fig. 1(a). The location of that particular surviving braid region can then be followed by tracking the streamwise displacement of the vertical line through the four phases. Of course, to continue tracking the surviving braid region beyond the location indicated by a line in Fig. 9(d), it is necessary to go back to Fig. 9(a) and follow the next downstream location indicated, and so on.

In order to investigate the spanwise scale of the rib structures, cross-stream (YZ) plane cuts through the selected surviving braid region are presented in Figs. 10(a-h) as this region evolves through the first, second, and third primary roller pairings. At $X = 7$ cm (Fig. 10a), approximately two pairs of streamwise vortex pairs are apparent, with the stronger pair on the left ($0 < Z < 2.5$ cm) and a weaker, less

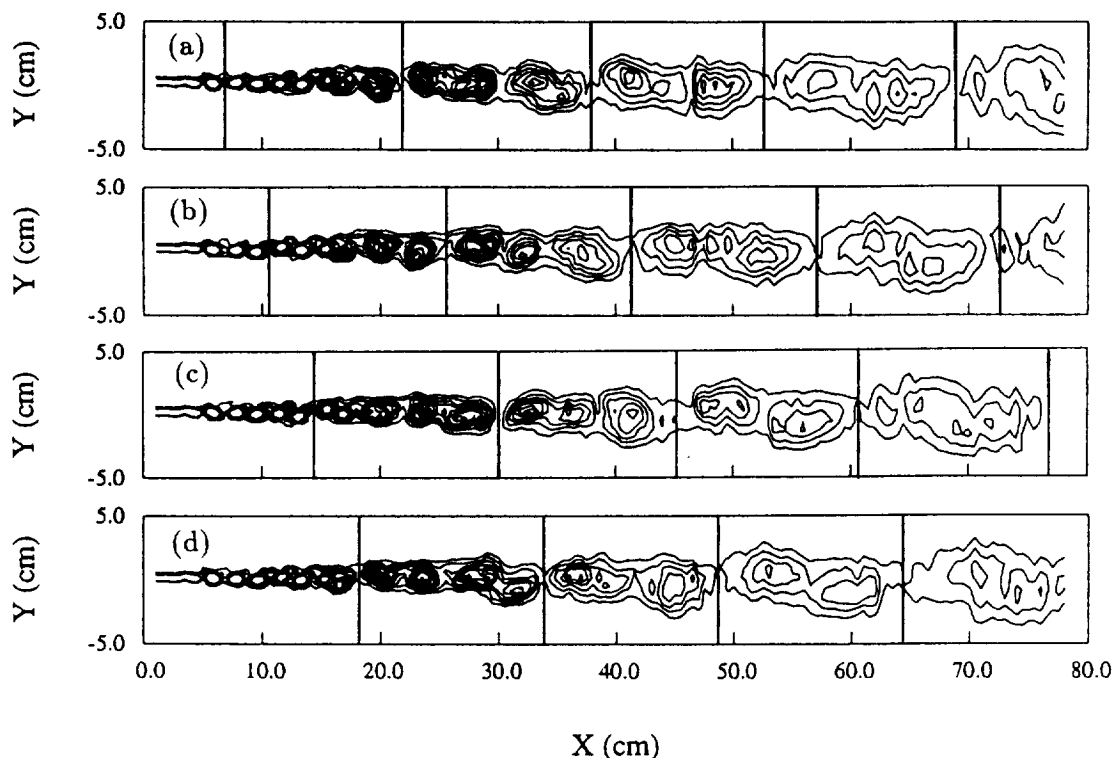


FIGURE 9. Centerplane phase-averaged spanwise vorticity ($\langle \Omega_z \rangle / U_0$, cm^{-1}) contours at various phases. Vertical lines mark the location of the surviving braid region tracked in Fig. 2. Lowest contour level = -0.113 , increment = -0.1 . (a) phase 1; (b) phase 9; (c) phase 17; (d) phase 25.

organized one on the right ($2.5 < Z < 5$ cm). In particular, the positive vortex at $Z \approx 3$ cm appears to be split into two smaller structures and the negative one at $Z \approx 4.5$ cm is considerably weaker than its counterpart at $Z \approx 2$ cm. The average spacing between the streamwise vortices is about 1.5 cm, which gives an initial spanwise to streamwise wavelength ratio of about 1.7. Further downstream, by $X = 17$ cm (Fig. 10b), the two weak positive structures have merged into one. Somewhat surprisingly, at $X = 18$ cm (Fig. 10c), the weak positive structure starts to split up again and the negative region above it has broken away from the stronger negative structure. Fig. 9(d) shows that at this location and phase, the selected braid region is right in the middle of the first roller pairing process. The upstream pair is in the process of rolling-up while the downstream pair has almost completely merged together.

Further downstream, the split positive pair merges together again and by $X = 25$ cm, at a time (phase) at which the braid is located between two paired rollers, two complete pairs of streamwise vortices are apparent (Fig. 10d). So while there is no scale change in the region of the first roller pairing as such, the weaker vortices do

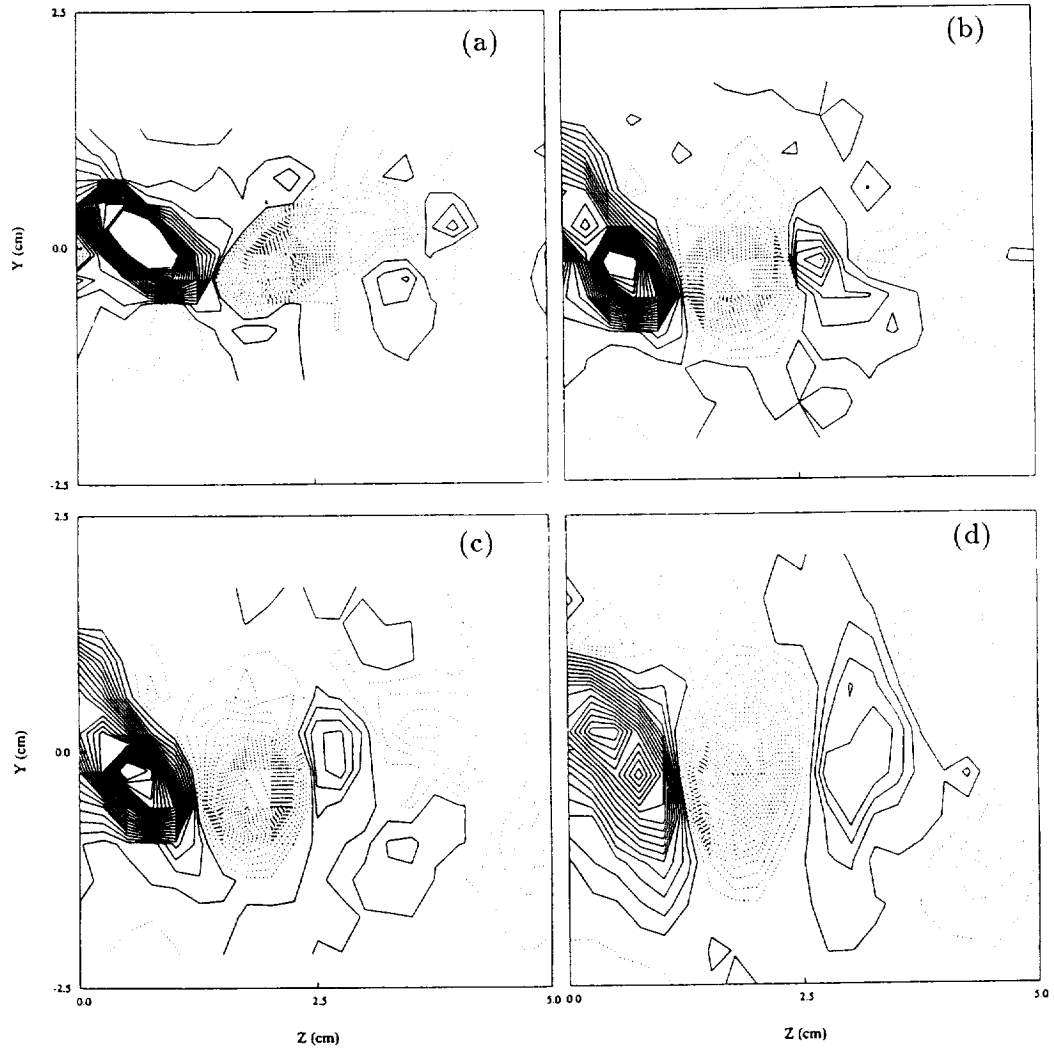


FIGURE 10. Cross-stream plane phase-averaged streamwise vorticity ($\langle \Omega_x \rangle / U_0$, cm^{-1}) contours. Negative \cdots , positive — , lowest level = ± 0.013 , increment = ± 0.025 . (a) $X = 7$ cm, phase 1; (b) $X = 17$ cm, phase 23; (c) $X = 18$ cm, phase 25; (d) $X = 25$ cm, phase 7.

undergo some temporary changes in structure and/or position. A similar behavior of the weaker vortices in this region was also observed in our two-frequency forcing results (LeBoeuf & Mehta 1994b).

The trends observed in the region of the first pairing continue during the second pairing. Following the weak positive vortex at $Z \approx 3$ cm, between $X = 25$ cm (Fig. 10d) and $X = 44.5$ cm (Fig. 10e), the vortex splits and recombines three more times. The split always occurs at the onset of an upstream or downstream

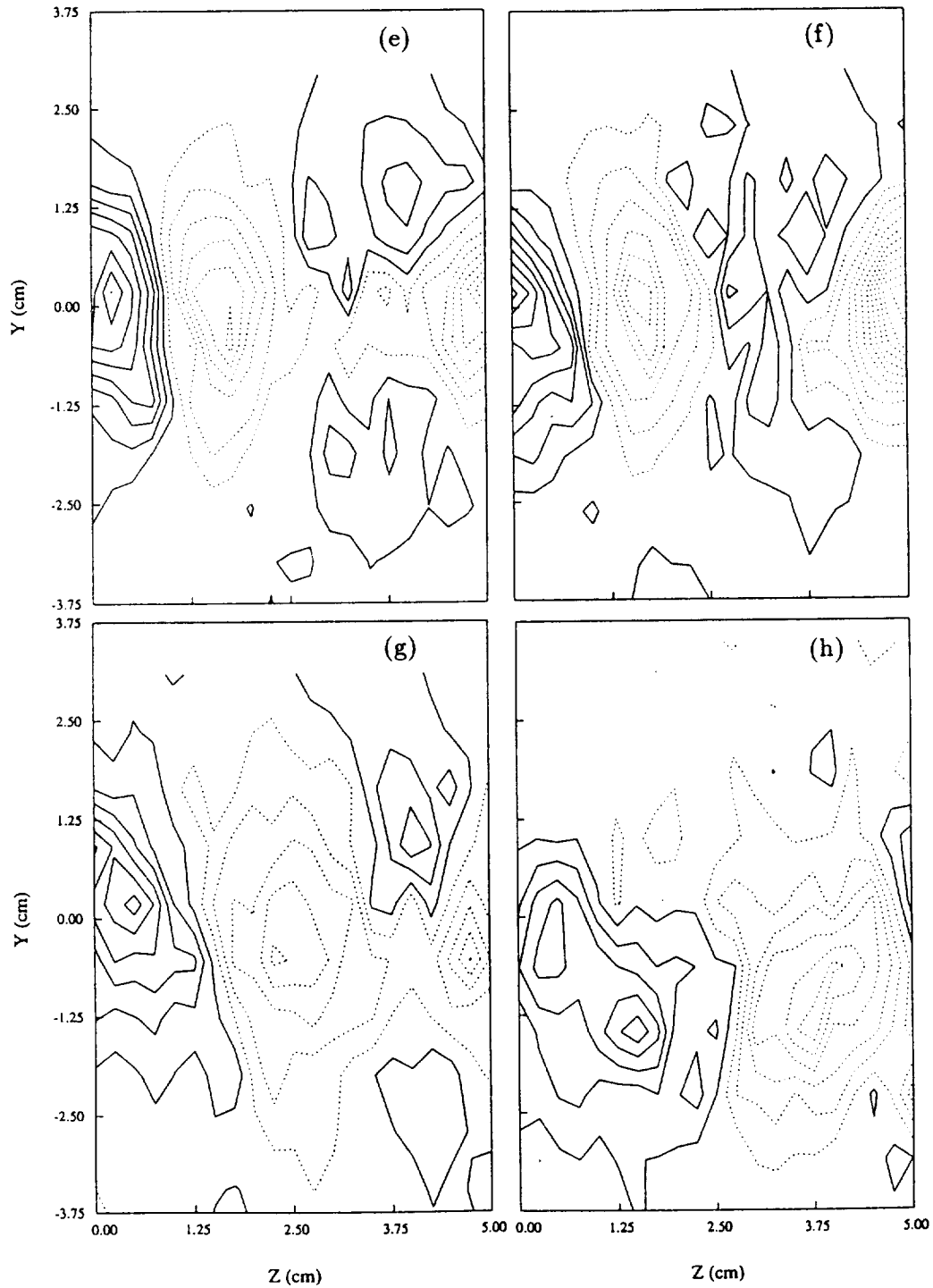


FIGURE 10 (CONTINUED). Cross-stream plane phase-averaged streamwise vorticity ($\langle \Omega_x \rangle / U_0$, cm^{-1}) contours. Negative \cdots , positive — , lowest level = ± 0.013 , increment = ± 0.025 . (e) $X = 44.5$ cm, phase 14; (f) $X = 46$ cm, phase 17; (g) $X = 48.5$ cm, phase 23; (h) $X = 57$ cm, phase 9.

roller pairing. The weak vortex at $Z \approx 3$ cm recombines for the last time at $X = 46$ cm during the beginning of the third pairing (Fig. 10*f*). Note that throughout its evolution through the first and second pairing, the stronger pair on the left ($0 < Z < 2.5$ cm) does not change much, except that the vorticity levels drop with streamwise distance as the vortices diffuse and thus enlarge. However, the enlargement only takes place in the vertical (Y) direction; the spanwise growth is presumably restricted by the neighboring streamwise vortices. In fact, the spacing between the two vortices *does not change* at all in the region, $X = 7$ to 46 cm.

By $X = 48$ cm (Fig. 10*g*), the weak positive vortex at $Z \approx 3$ cm splits again, but this time the two neighboring negative vortices move closer together into the area vacated by the weak positive vortex and start to amalgamate. The fragments of the shredded positive vortex appear to move out of the measurement domain. At $X = 57$ cm (Fig. 10*h*), only a *single* pair of streamwise vortices is clearly visible with the distance between the pair *doubled*. This single pair persists to the end of the measurement domain ($X = 78$ cm). The spacing between the pair is about 3.6 cm, which gives a spanwise to streamwise wavelength ratio of about 0.5.

Clearly the mechanism for the increase in spanwise scale is that the weakest (positive) vortex splits up and moves out of the array, the two neighboring vortices (both negative) move closer together and amalgamate, and the spanwise spacing is hence readjusted. Apparently there was a tendency for the weakest vortex to split and thereby permit merging of the two like-signed adjacent vortices during both the first and second pairing; however, the merging finally occurred during the third primary roller pairing. If this was a true amalgamation of two vortices of the same sign, then one would expect the circulation of the new (merged) vortex to be higher than those of the original vortical structures. And indeed, in the present results, the circulation of the merged negative structure in Fig. 10(*h*) is twice that of one of the original negative structures (that at $Z \approx 2$ cm in Fig. 10*f*).

In order to confirm that the observed scale change was not an artifact of the imposed forcing signal, time-averaged streamwise vorticity measurements for the forced mixing layers (averaged over all 32 phases) were compared to those obtained in the same mixing layer, but with the forcing turned off. All other initial and operating conditions were maintained exactly the same in this *unforced* mixing layer. In both cases, the spanwise scale observed in the mean streamwise vorticity measurements was constant out to $X \approx 50$ cm, after which it doubled abruptly. Therefore, the forcing is obviously *not* responsible for the location of the observed scale change.

The present results agree, in particular, with many of the observations and notions of Bell & Mehta (1992) developed from their time-averaged measurements. They also observed the first rapid scale change at $X \approx 50$ cm, which was estimated to be the location of the third roller pairing. As in the present study, the spanwise scale was found to double in this region. Since the locations of the scale changes were correlated with local increases in the average streamwise circulation per vortex, Bell & Mehta suggested that the mechanism for the increase in spanwise scale was amalgamation of vortices of the same sign, which is exactly what is observed here.

Tung (1992) also reported seeing some (local) pairings of streamwise vortices of the same sign. While the other proposed mechanisms, such as viscous annihilation and amalgamation of opposite sign vortex pairs (Jimenez 1983, Rogers & Moser 1993), have not been observed in the present direct measurements, in principle there is no reason why they should not occur, providing the local circumstances (such as streamwise vortex strength and spacing, for example) are right.

The balance of experimental evidence suggests that the spanwise wavelength of the streamwise structures will increase, scaling approximately with the mixing layer vorticity thickness. However, the increase will in general be non-linear (stepwise) with the jumps coinciding with *some* pairing locations. An increase in spanwise wavelength has not been observed experimentally in the absence of spanwise roller pairings. However, it is quite clear that the spanwise scale does not have to increase at every spanwise roller pairing location, although it can, as shown by Huang & Ho (1990). This means that, in general, a constant ratio of spanwise to streamwise wavelength will not be maintained. At least one (measured) mechanism for the increase in spanwise scale is amalgamation of streamwise vortices of the same sign. As Rogers & Moser (1993) suggested, in practice the details of the spanwise scale change will probably be determined by the incoming disturbance environment.

Part 2: Forced wake

1. Motivation and objectives

The effects of (passive) spanwise perturbations on the wake three-dimensionality have been investigated in a few studies. Meiburg & Lasheras (1988) investigated the structure of a perturbed splitter plate wake through inviscid vortex simulations and low Reynolds number flow visualization experiments and found that the redistribution, reorientation, and stretching of vorticity produced counter-rotating pairs of streamwise vortices which were superimposed onto the spanwise vortices. These streamwise vortices were in the form of lambda-shaped structures and resided in the braid regions connecting adjacent (opposite-signed) spanwise vortices. Subsequent interaction of the streamwise and spanwise structures led to the formation of closed vortex loops.

Although the secondary structure in a plane wake has already received some attention both experimentally and computationally, all issues regarding the three-dimensional structure of a wake developing from “natural” initial conditions have not yet been addressed. The appearance of mean streamwise vorticity in time-averaged measurements confirmed the existence of coherent spatially-stationary secondary vorticity in wakes (Weygandt & Mehta 1993). However, the details of the secondary structure are lost through the averaging process. The popular use of Taylor’s hypothesis in the past in interpreting three-dimensional measurements can obviously add to the uncertainty. As for the computations, limits imposed by boundary conditions and the expense associated with grid size and computation time make it difficult to evaluate the structure of a “natural” spatially-developing wake.

The main objective of this study was to investigate the formation of three-dimensionality and its evolution in a forced plane wake developing from laminar boundary layers. Acoustic forcing was used to phase-lock the shedding of the Karman vortices. Phase-averaged measurements were then used to quantify the resulting vorticity development and interaction. These measurements, coupled with previous experimental and simulation results, shed new light on the structural development of spatially-evolving wakes with "natural" initial conditions (LeBoeuf & Mehta 1994*d*).

2. Accomplishments

2.1 The experiment

The experiments were conducted using the same equipment as that used for the aforementioned mixing layer experiments. Therefore a complete description will not be repeated here. Of course, there were differences in operating conditions, namely that the two sides of the wake were set to 9 m/s and the forcing consisted of a single sine wave at the fundamental roll-up frequency (450 Hz, obtained from centerline spectra in the unforced wake). The boundary layers on the splitter plate were laminar and nominally two-dimensional at these operating conditions. Again, the amplitude of the output signal from the amplifier was set to the absolute minimum level which still gave adequate coherence in the phase-locking.

For the phase-averages shown in the next section, 768 ensembles of 16 samples per cycle were measured. The measurement grid consisted of 29 uniformly spaced X locations in the range 1 to 15 cm and 20 uniformly spaced Y locations distributed over a linearly increasing range of -1 to 1 cm at $X = 1$ cm to -1.8 to 1.8 cm at $X = 15$ cm. In the spanwise direction, the three-dimensional grid ranged from $Z = -5$ to 5 cm with 41 uniformly spaced locations, thus occupying the central ninth of the total test section span.

2.2 Results and discussion

The streamwise evolution of phase-averaged spanwise vorticity ($\langle \Omega_z \rangle / U_e$, cm^{-1}) along the wake centerline ($Z = 0$) is depicted in Figs. 11(*a-d*) for four phases (or times). In effect, every fourth phase out of the 16 measured phases per forcing cycle is presented. The formation and evolution of the two rows of opposite-signed vortices forming the familiar Karman street can be easily tracked through the four phases shown. The initial spanwise instability leading to the first spanwise vortex roll-up occurs at $X \approx 3$ cm. This coincides with the location at which significant streamwise vorticity was first measured.

Details of the vortical structures were examined more closely by using two-dimensional "cuts" through the three-dimensional data. The first signs of any significant streamwise vorticity at phase 1 were found at $X = 3$ cm. This location is just *upstream* of the first positive spanwise roller, which at this phase has not yet peeled away from the initial shear layer (see Fig. 11*a*). It also coincides with the location where the instability leading to the formation of the spanwise rollers first appears. The fact that significant streamwise vorticity is not measured in the

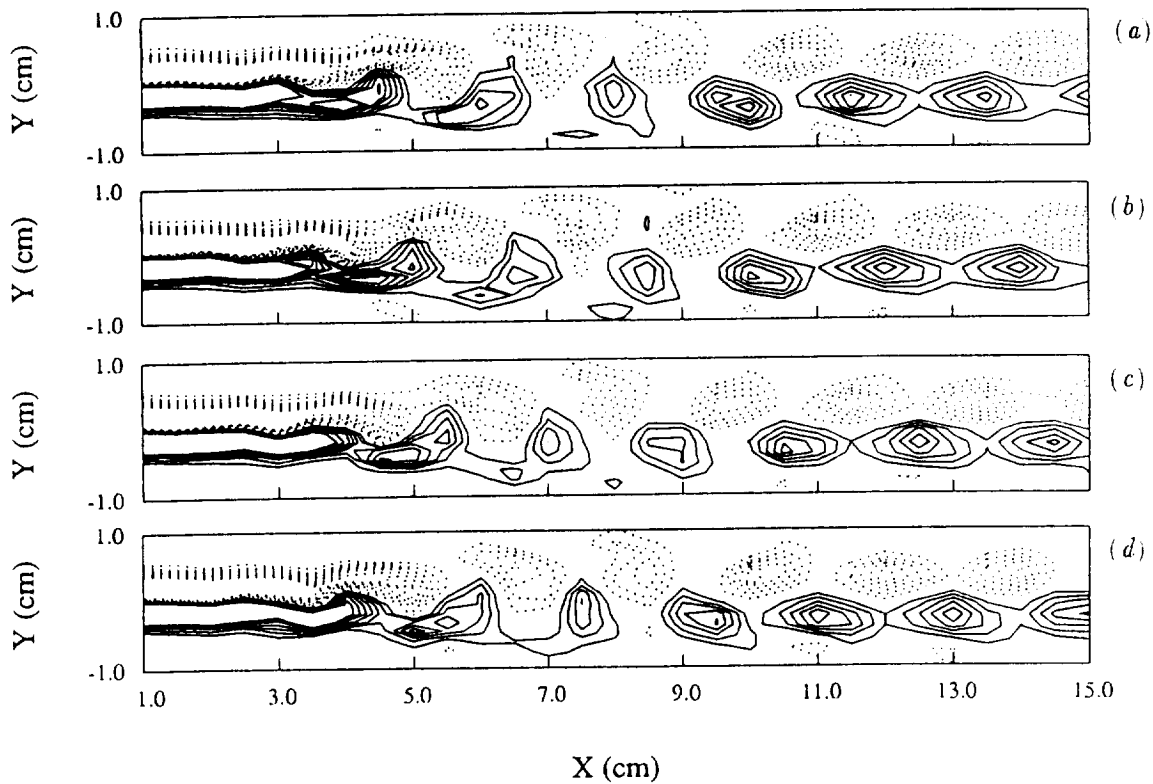


FIGURE 11. Centerplane phase-averaged spanwise vorticity ($\langle \Omega_z \rangle / U_e$, cm^{-1}) contours at various phases. Lowest level = ± 0.15 , increment = ± 0.15 . (a) phase 1; (b) phase 5; (c) phase 9; (d) phase 13.

very near-field region ($1 < X < 2.5$ cm) of the present wake supports the view that the appearance of streamwise vorticity further downstream is due to an amplification of weak incoming disturbances — it is not just a simple case of *relatively strong* streamwise vorticity being fed in directly from the boundary layers. In this study, perceptible amplification occurs as soon as the first spanwise vortices start to roll up. Since the (upstream) braid undergoes streamwise stretching during this phase, it is presumed that this is the mechanism by which weak incoming disturbances (weak longitudinal vortices) are amplified. Details of the initial streamwise structures are not uniform across the span because the “natural” disturbance environment of the incoming flow field is not expected to be uniform.

In order to investigate the incoming disturbance field and initial formation region in more detail, the cross-stream plane streamwise vorticity contours at $X = 3$ cm are presented in Figs. 12(a) and (b) for phases 5 and 9. These figures show that the incoming disturbance field is in the form of an approximate single row of counter-rotating streamwise vortices whose cross-stream (Y) location changes with phase. On comparing Figs. 12(a) and (b), which are exactly one half cycle apart, it is evident that a single row appears on the lower half of the wake at phase 5, but on

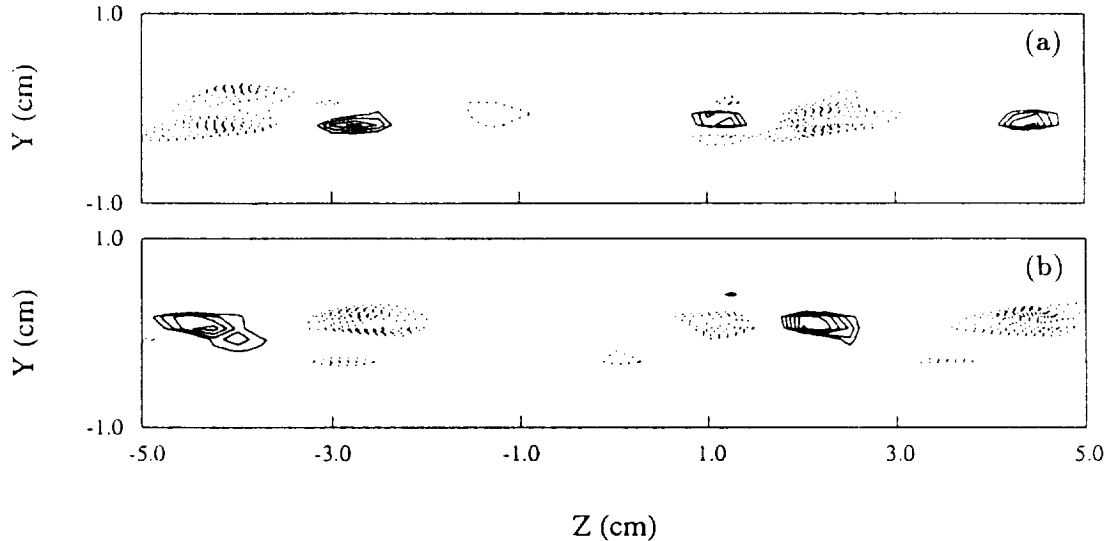


FIGURE 12. Phase-averaged streamwise vorticity ($\langle \Omega_x \rangle / U_e$, cm^{-1}) contours at $X = 3$ cm for various phases. Negative \cdots , positive — , lowest level = ± 0.015 , increment = ± 0.05 . (a) phase 5; (b) phase 9.

the upper half at phase 9. On inspecting Figs. 11(b) and (d), it is apparent that at phase 5 the lower spanwise vortex is rolling-up prior to shedding, whereas at phase 9 the same situation is true for the upper roller. So it appears as though disturbances from both boundary layers are fed into the wake and amplified. At a given phase, depending on which (positive or negative) spanwise vortex is rolling up, the disturbances fed into that vortex sheet are amplified as the sheet is stretched. Thus, an alternating-signed array of streamwise vorticity is generated for every half cycle. This explains why the time-averaged measurements of Weygandt & Mehta (1993) exhibited two rows of mean streamwise vorticity arranged in quadrupoles.

The alternating-signed inlet streamwise vorticity development for every half cycle is characteristic of the “mode 2” disturbance field of Lasheras & Meiburg (1990). In their simulations, this mode resulted in out-of-phase undulations of the primary rollers. These roller distortions were easily recognizable in the current data set. For example, their imprint was evident in YZ -plane contours of streamwise velocity (not shown here), which exhibited a pinching and cresting behavior in the spanwise direction. The same type of behavior was also noted by Weygandt & Mehta (1993) in their mean velocity contours.

It is not clear from the present study if it will always be the alternating-signed streamwise vorticity of mode 2 that is generated when the wake develops from “natural” laminar boundary layers. It has been shown in both simulations and experiments that the “mode 1” perturbation can also be sustained if the corresponding disturbance field is introduced at the wake origin (Buell & Mansour 1989b; Lasheras

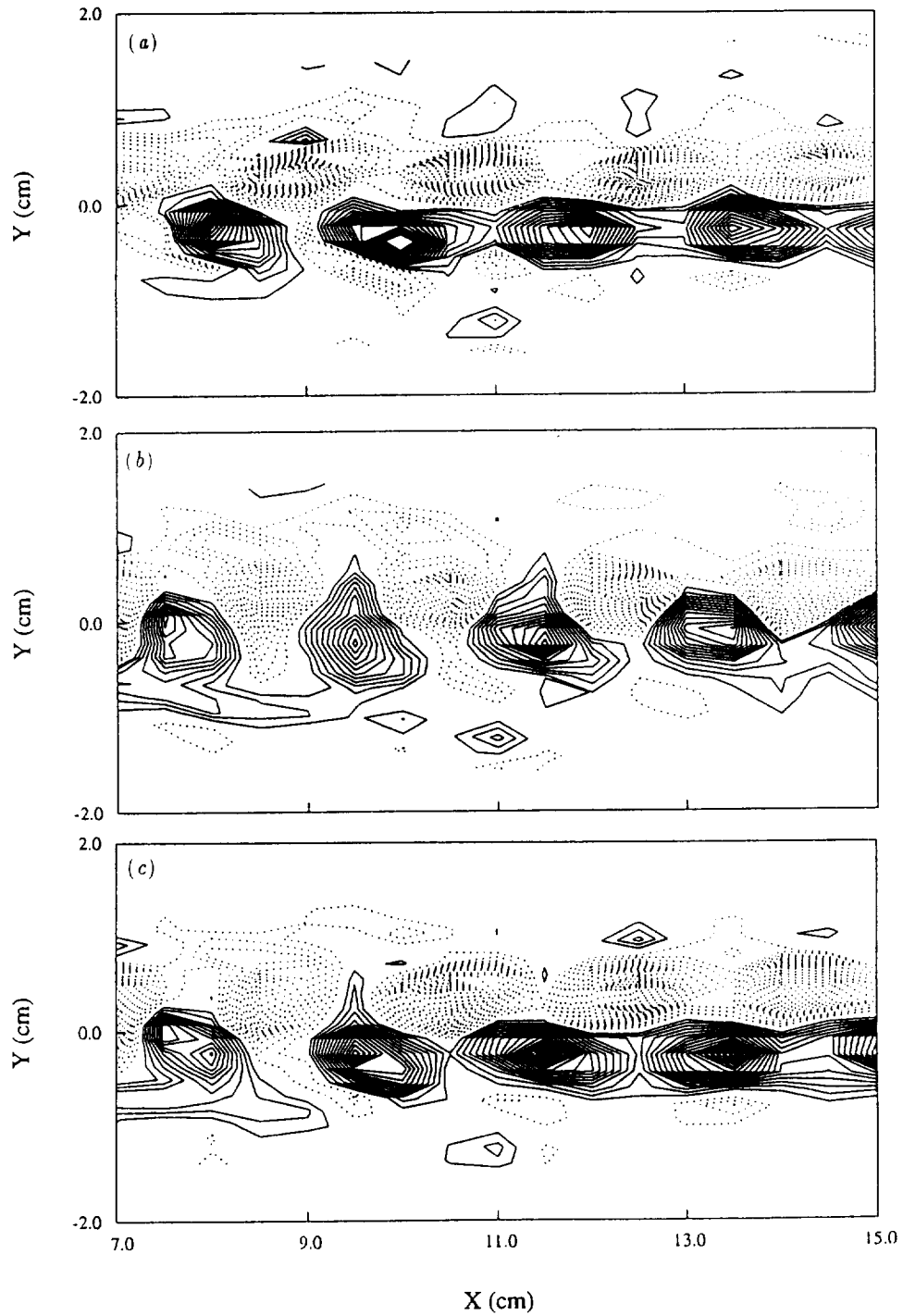


FIGURE 13. Phase-averaged spanwise vorticity ($\langle \Omega_z \rangle / U_e, \text{cm}^{-1}$) contours at phase 1. Negative \cdots , positive --- , lowest level = ± 0.05 , increment = ± 0.05 . (a) Cut through a rib at $Z = 2.25$ cm; (b) Cut through a region between ribs, $Z = 3.25$ cm; (c) Cut through a rib at $Z = 4.25$ cm.

& Meiburg 1990). The mode 1 disturbance field consists of the same-signed streamwise vorticity for every half-cycle and leads to an in-phase undulation of the primary rollers. In the present study, the results suggest that disturbances from both boundary layers are fed into the wake as discussed above. It is fair to assume that, at least upstream of the splitter plate trailing edge, the disturbance fields in the two boundary layers are fully independent of each other. So it is either a coincidence that the inlet disturbance field corresponds to mode 2, or there must be some realignment of the disturbances in the region immediately downstream of the splitter plate trailing edge ($0 < X < 3$ cm) which reorganizes a random field into one corresponding to mode 2. Since the initial disturbance field is typically too weak to measure directly, this issue cannot be easily settled in experimental studies.

In order to examine the details of the vorticity morphology, longitudinal (XY) cuts in the Karman vortex street region ($X = 7$ to 15 cm) showing spanwise and streamwise vorticity contours are presented in Figs. 13 and 14, respectively. The XY -planes are chosen based on the spanwise locations of the streamwise structures, as shown, for example, in the cross-stream contours of streamwise vorticity included as Fig. 15. Two of the planes cut through adjacent rib structures at $Z = 2.25$ cm (Figs. 13*a* and 14*a*) and 4.25 cm (Figs. 13*c* and 14*c*) and the third ($Z = 3.25$ cm) represents the plane in between the two streamwise structures (Figs. 13*b* and 14*b*).

Of course, in the plane between the legs of the loops ($Z = 3.25$ cm), no significant streamwise vorticity is measured (Fig. 14*b*). However, in the rib-planes, it is clear from Figs. 14(*a*) and (*c*) that apart from rib vorticity connecting the spanwise rollers, the rollers themselves also make a significant contribution to the streamwise vorticity. This is a result of the rollers becoming kinked (along the span) in the streamwise direction. Note that on a given side of the wake (positive or negative Y), the streamwise vorticity contribution due to roller kinking is of opposite sign to that of the ribs. This effect has also been noted in numerical simulations of wakes (Buell & Mansour 1989*b*), and it is attributed to vortex stretching terms in the streamwise vorticity equation (Buell 1991). The streamwise vorticity due to the roller kinking is staggered relative to the ribs in the Y -direction, thus forming the four-tier structure observed in YZ -planes (Fig. 15).

The main difference between the cuts at $Z = 2.25$ cm and $Z = 4.25$ cm is that regarding the sign of the ribs; the upper ribs are negative and the lower ribs are positive in Fig. 14(*a*) whereas in Fig. 14(*c*) the upper ribs are negative and the lower positive. This configuration strongly suggests the vortex loop structure proposed by Lasheras & Meiburg (1990) for their mode 2 perturbation. If the present three-dimensional structure indeed consists of vortex loops, then the "heads" of the loops should be visible in the spanwise vorticity contours at $Z = 3.25$ cm, the plane separating the rib structures at $Z = 2.25$ and $Z = 4.25$ cm. Small spanwise vorticity peaks, relative to the primary Karman vortex street, are certainly discernible in Fig. 13(*b*). It is noteworthy that the peaks appear on *both* sides of the wake, implying that it is indeed the mode 2 configuration — the mode 1 perturbation would only produce peaks on one side of the wake. Local spanwise vorticity peaks are also observed in Figs. 13(*a*) and (*c*), the planes cutting through the rib vortices.

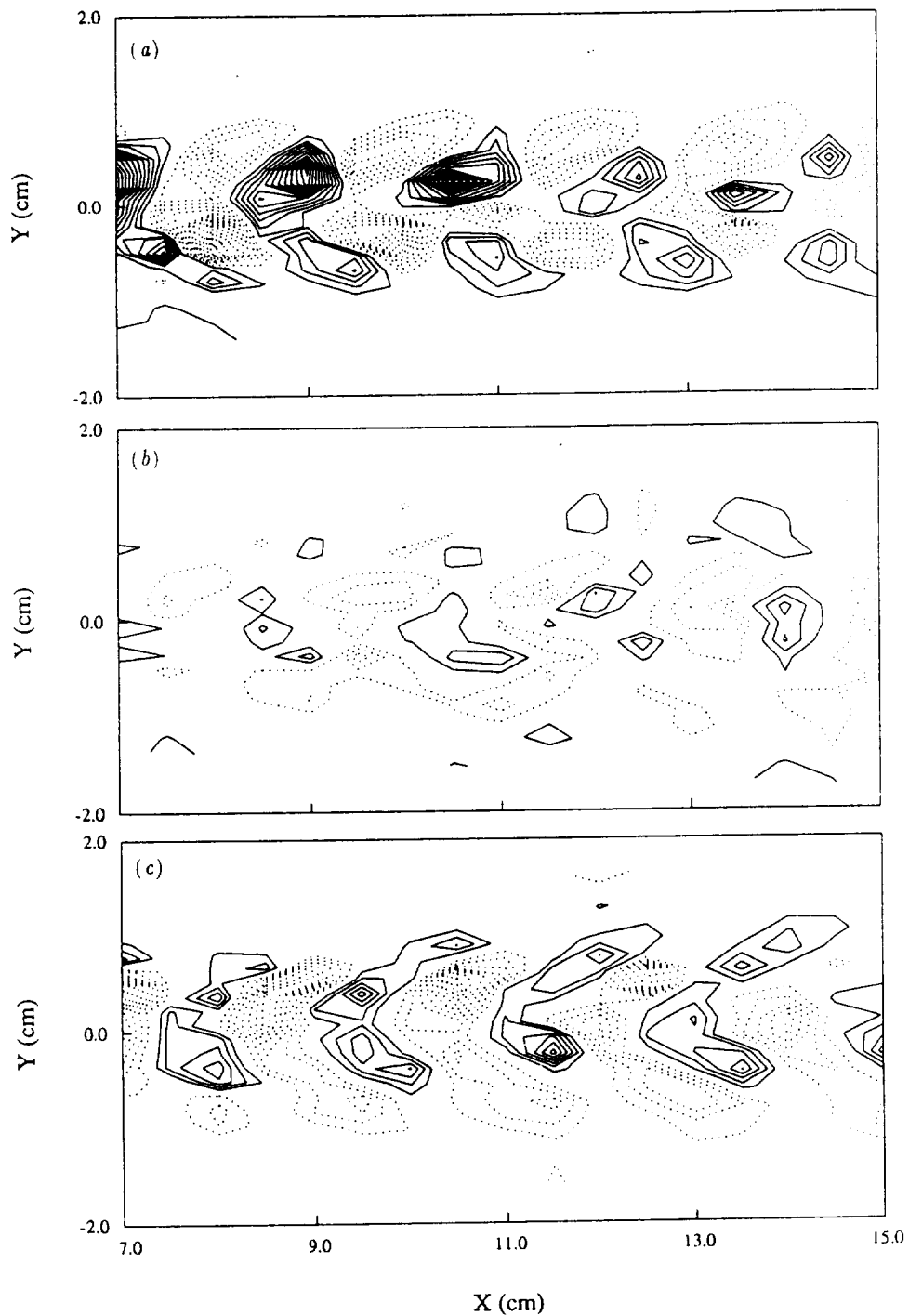


FIGURE 14. Phase-averaged streamwise vorticity ($\langle \Omega_x \rangle / U_e$, cm^{-1}) contours at phase 1. Negative \cdots , positive — , lowest level = ± 0.05 , increment = ± 0.05 . (a) Cut through a rib at $Z = 2.25$ cm; (b) Cut through a region between ribs, $Z = 3.25$ cm; (c) Cut through a rib at $Z = 4.25$ cm.

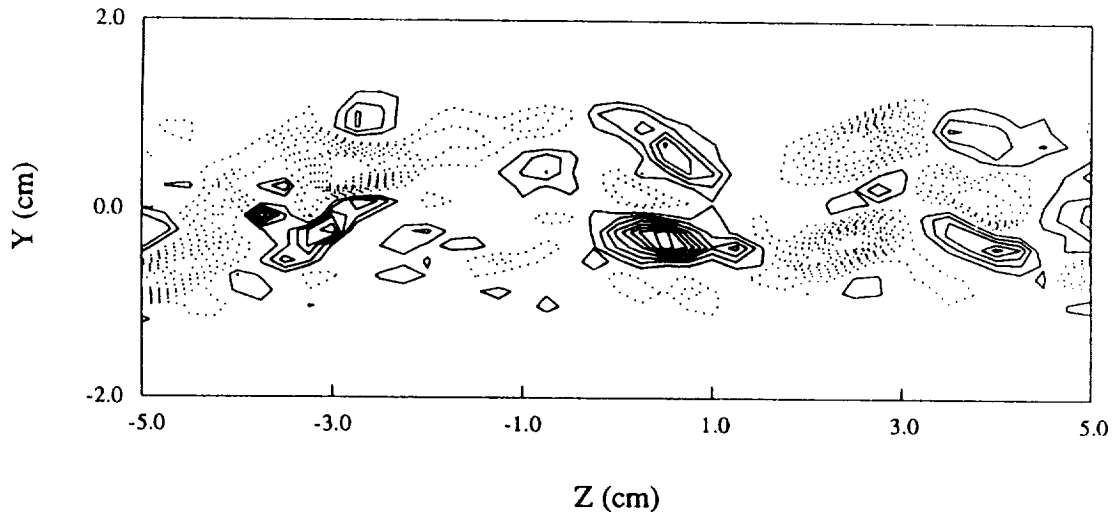


FIGURE 15. Cross-stream plane phase-averaged streamwise vorticity ($\langle \Omega_x \rangle / U_e$, cm^{-1}) contours in the Karman vortex street region at phase 1 and $X = 10$ cm. Negative , positive ——— , lowest level = ± 0.05 , increment = ± 0.05 .

This observation implies that the ends of the vortex loops wrapping around the spanwise rollers are inclined in the spanwise direction.

The present results clearly show that a plane wake originating from laminar boundary layers will develop a three-dimensional structure in the form of streamwise vorticity as soon as the primary instability generates spanwise vortex rollers. The secondary structure takes the form of vortex loops which connect opposite-signed spanwise rollers. The details of the vortex loop structures are dependent on the initial disturbance field. This secondary structure topology forms an integral and important part of a transitioning wake, and it must be accounted for in all modeling and wake control studies.

Acknowledgements

This work was performed in the Fluid Mechanics Laboratory, NASA Ames Research Center in collaboration with Dr. R. D. Mehta. We are grateful to Drs. R. D. Moser and M. M. Rogers for many helpful discussions. We would like to thank Dr. J. H. Watmuff for sharing his digital sine-wave generator design and also for many invaluable suggestions.

REFERENCES

- BELL, J. H. AND MEHTA, R. D. 1992 Measurements of the streamwise vortical structures in a plane mixing layer. *J. Fluid Mech.* **239**, 213.
- BUELL, J. C. 1991 A hybrid numerical method for three-dimensional spatially-developing free-shear flows. *J. Comp. Phys.* **95**, 313-338.

- BUELL, J. C. & MANSOUR, N. N. 1989a Asymmetric effects in three-dimensional spatially-developing mixing layers. *Proc. Seventh Symp. Turbulent Shear Flows, Stanford University, August, 9.2.1-9.2.6.*
- BUELL, J. C. & MANSOUR, N. N. 1989b Near-field structures in three-dimensional spatially-developing wakes. *Proc. Tenth Australasian Fluid Mechanics Conference, Melbourne, Australia, 9.21-9.24.*
- HUANG, L. S. & HO, C. M. 1990 Small-scale transition in a plane mixing layer. *J. Fluid Mech.* **210**, 475-500.
- JIMENEZ, J. 1983 A spanwise structure in the plane mixing layer. *J. Fluid Mech.* **132**, 319-326.
- LASHERAS, J. C. & CHOI, H. 1988 Three-dimensional instability of a plane free shear layer: an experimental study of the formation and evolution of streamwise vortices. *J. Fluid Mech.* **189**, 53-86.
- LASHERAS, J. C. & MEIBURG, E. 1990 Three-dimensional vorticity modes in the wake of a flat plate. *Phys. Fluids A.* **12**, 371-380.
- LEBOEUF, R. L. 1993 Vortical structure in a forced plane mixing layer. *Annual Research Briefs - 1993*, Center for Turbulence Research, NASA Ames Research Center - Stanford University, 285-298.
- LEBOEUF, R. L. & MEHTA, R. D. 1994a On using Taylor's hypothesis for three-dimensional mixing layers. Submitted to *Phys. Fluids*.
- LEBOEUF, R. L. & MEHTA, R. D. 1994b Vortical structure morphology in a forced mixing layer: initial roll-up and pairing. Submitted to *J. Fluid Mech.*
- LEBOEUF, R. L. & MEHTA, R. D. 1994c Measurements of spanwise scale change in a forced mixing layer. Submitted to *J. Fluid Mech.*
- LEBOEUF, R. L. & MEHTA, R. D. 1994d Topology of the near-field vortical structures in a three-dimensional wake. Submitted to *J. Fluid Mech.*
- MEIBURG, E. & LASHERAS, J. C. 1988 Experimental and numerical investigation of the three-dimensional transition in plane wakes. *J. Fluid Mech.* **190**, 1-37.
- MOSER, R. D. & ROGERS, M. M. 1993 The three-dimensional evolution of a plane mixing layer: pairing and transition to turbulence. *J. Fluid Mech.* **247**, 275-320.
- NYGAARD, K. J. & GLEZER, A. 1991 Evolution of streamwise vortices and generation of small-scale motion in a plane mixing layer. *J. Fluid Mech.* **231**, 257-301.
- ROGERS, M. M. & MOSER, R. D. 1991 The three-dimensional evolution of a plane mixing layer. Part 1. The Kelvin-Helmholtz rollup. *NASA T-M 109856.*
- ROGERS, M. M. & MOSER, R. D. 1992 The three-dimensional evolution of a plane mixing layer: the Kelvin-Helmholtz rollup. *J. Fluid Mech.* **243**, 183-226.
- ROGERS, M. M. & MOSER, R. D. 1993 Spanwise scale selection in plane mixing layers. *J. Fluid Mech.* **247**, 321-337.

- TUNG, C. H. 1992 Initial streamwise vorticity formation in a two-stream mixing layer. *PhD Dissertation*, University of Houston.
- WEYGANDT, J. H. & MEHTA, R. D. 1993 Three-dimensional structure of straight and curved plane wakes.. *JIAA Rep. TR-110*. Dept. of Aeronautics and Astronautics, Stanford University. Shortened version to appear in *J. Fluid Mech.*